ADVANCED MATERIALS
www.advmat.de

www.MaterialsViews.com

Completely Organic Multilayer Thin Film with Thermoelectric Power Factor Rivaling Inorganic Tellurides

*Chungyeon Cho, Bart Stevens, Jui-Hung Hsu, Ricky Bureau, David A. Hagen, Oren Regev, Choongho Yu, and Jaime C. Grunlan**

The majority of energy produced is dissipated into the environment as waste heat (4100 TW h per year in the United States),[1] but this could become a significant source of useful energy using thermoelectric (TE) materials that directly convert waste heat into voltage.[2,3] TE systems are expected to play an increasingly important role in meeting our future energy needs because they can harvest electricity from low-quality heat sources with no moving mechanical components, ensuring high reliability.[4,5] The efficiency of a TE material is often expressed in a dimensionless figure-of-merit ($ZT = S^2\sigma T\kappa^{-1}$), where S is the Seebeck coefficient, σ is the electrical conductivity, κ is the thermal conductivity, and T is the absolute temperature. It is clear that a material should possess a high S and σ, along with a low κ to obtain a high ZT value, but the strong interdependence of these parameters (increasing σ is usually accompanied by an increased κ and decreased S) makes optimization challenging.[6]

The most efficient TE materials are inorganic semiconductors, such as lead and bismuth telluride (the latter has $ZT \approx 1$ at room temperature).[7–9] Despite their promise, these inorganic materials have significant drawbacks that include the high cost of raw materials, toxicity, shortage of natural resources (Te is one of the rarest elements on earth), poor processability, and potential for heavy metal pollution, which hinders their widespread use.[4,10] It is for these reasons that increasing attention is being paid to organic TE materials.[11] This unique new class of TEs offers the potential to be low cost (due to abundance of carbon), easy to process (can be painted or printed), and environmentally benign. In most cases, these organics are polymer based, so they exhibit low thermal conductivity, which is ideal for TE efficiency. TE properties of organics are still inferior to those of conventional inorganics, primarily due to low σ and S, but nanocomposites incorporating carbon nanotubes or graphene, along with intrinsically conducting polymers such as polyaniline (PANi), have shown reasonably good electrical transport and are very promising candidates.[12]

The best TE nanocomposites require graphene and/or nanotubes to be well dispersed in a polymer matrix, but it is very difficult to homogenously disperse through simple mixing,[13] one-pot fabrication,[14] creation of porous core/shell nanocomposites,[15] or polymer emulsions.[16] In some cases, a template-directed in situ polymerization is an effective method to construct well-dispersed polymer/organic nanocomposites, but the obtained TE performance is far below that of inorganic-based composites.[17] In this regard, layer-by-layer (LbL) assembly offers several advantages over other fabrication methods for ordered thin films. LbL assembly is a simple and versatile method to make highly tunable and conformal multifunctional films through sequential exposure of a substrate to aqueous solutions containing complementarily functionalized materials.[18–20] Nanocomposites can be produced via LbL with nanometer-scale control of structure and composition.[21–23] There are a few reports in which TE properties of organic/inorganic composites assembled by an LbL method are identified.[24–26] However, relatively little work concerning TE LbL assemblies has involved enhancing the power factor, and to our knowledge no detailed qualitative and quantitative measurements of TE performances of the organic multilayer composites have been reported. In the present study, ordered polyelectrolyte carbon nanocomposites (PCNs) were deposited via sequential layering of PANi, graphene, and double-walled carbon nanotubes (DWNT). This unique combination resulted in increased carrier mobility, originating from strong π–π interactions between PANi and DWNT and the higher electrical conductivity of graphene. In this investigation of the TE behavior of an LbL-assembled film, the resulting PCN exhibits a remarkable power factor (PF ($S^2\sigma$) = 1825 μW m^{-1} K^{-2}) that exceeds lead telluride and is more than half the value of bulk bismuth telluride.[27,28]

Figure 1a shows the thickness profile of PANi/graphene, PANi/DWNT, and PANi/graphene/PANi/DWNT multilayers deposited on a Si-wafer using LbL deposition. For the bilayer (BL) assemblies, DWNT (diameter 2–3 nm), stabilized with negatively-charged sodium dodecylbenzenesulfonate (SDBS), or graphene, stabilized with poly(4-stryrenesulfonic acid) (PSS), was assembled with cationic PANi at pH 2.5. The PANi solution was carefully filtered so as to remove any un-dissolved solids and the prepared solution was used within a week due to its susceptibility to precipitation (see Supporting Information for experimental details).[29] Both PANi/graphene and PANi/DWNT BLs exhibit linear growth with an average thickness of 4.8 and 6.3 nm per BL, respectively. PANi/DWNT

Dr. C. Cho, B. Stevens, R. Bureau, D. A. Hagen, Prof. C. Yu, Prof. J. C. Grunlan
Department of Mechanical Engineering
Texas A&M University
College Station, TX 77843–3123, USA
E-mail: jgrunlan@tamu.edu
J.-H. Hsu, Prof. C. Yu, Prof. J. C. Grunlan
Department of Material Science and Engineering
Texas A&M University
College Station, TX 77843–3003, USA
Dr. O. Regev
Department of Chemical Engineering
Ben-Gurion University of the Negev
Beer-Sheva 8410501, Israel

DOI: 10.1002/adma.201405738

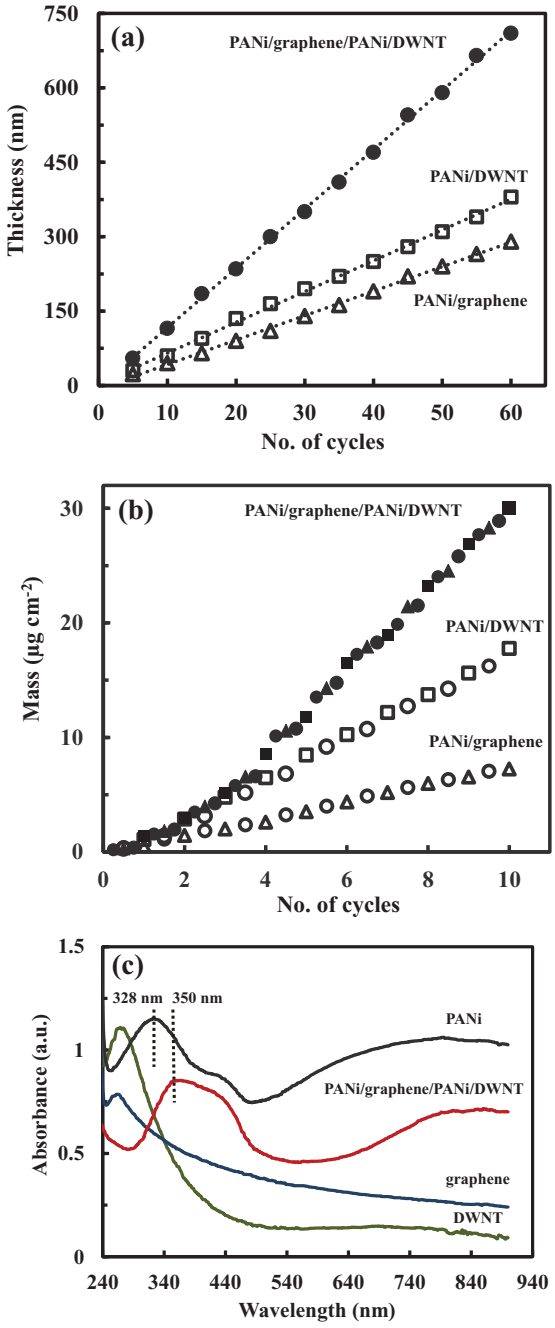

Figure 1. a) Thickness and b) mass growth of PANi/graphene, PANi/DWNT, and PANi/graphene/PANi/DWNT as a function of bilayers and quadlayers (i.e., cycles) deposited. c) UV–vis spectra of aqueous DWNT, graphene, and PANi solutions and a 4 PANi/graphene/PANi/DWNT QL film.

PCN grows thicker than the graphene-based films due to the more 3D structure of the nanotubes. Quadlayer (QL) films of PANi/graphene/PANi/DWNT exhibit a thickness per QL that is close to the sum of the individual BL systems (11.8 nm per QL), suggesting uniform and well-controlled assembly of these layers. Similar to the trend observed with the film thickness, mass deposited of these PCN systems, as measured using a quartz crystal microbalance (QCM), is linearly proportional to the number of BL or QL deposited, demonstrating a constant composition during the assembly (Figure 1b). When taken together, profilometer and QCM analysis allow the density and composition of these thin films to be calculated. The density of PANi/DWNT (2.75 g cm^{-3}) is higher than PANi/graphene (1.61 g cm^{-3}), suggesting that the DWNT-based assembly has a more tightly packed nanostructure. For QL–PCN, the concentration of each component was determined to be 37.7, 21.4, and 40.9 wt% for PANi, graphene, and DWNT, respectively, resulting in a film density of 2.49 g cm^{-3}. Although the mass growth of QL–PCN was measured within 10 cycles, the concentration of each component is speculated to be constant at 40 cycles because of its linearly growing characteristic.

Figure 1c shows UV–vis spectra of DWNT, graphene, PANi, and 4 QL of PANi/graphene/PANi/DWNT. PANi exhibits two characteristic absorbance peaks at 328 and 430 nm and a broad band beyond 700 nm, which are assigned the π–π^* transition of benzenoid rings, polaron–π^* transitions (a typical characteristic of the conducting emeraldine state of PANi), and π–polaron transitions, respectively.[30,31] After assembling into a nanocomposite film, the DWNT and graphene absorption bands near 270 nm were not observed, which is likely due to the overlap with the spectral signal of PANi. The PANi benzenoid peak was red-shifted by 22 nm in comparison to that of the neat PANi solution. This shift toward higher wavelength is closely correlated with the extension of conjugation caused by the strong π–π interaction of PANi oriented along the DWNT. Additionally, the large surface area of the graphene may serve as a conducting bridge to connect PANi–DWNT conducting domains, which improves percolation and reduces the energy for the electronic transition. These behaviors suggest that the conformation of PANi changes to a further expanded (more uncoiled) form, reducing the π defects caused by ring twisting and strengthening the π–π conjugation interactions between rings in the PANi/graphene/PANi/DWNT PCN. Therefore, the degree of charge delocalization of carriers along the backbone chain in the 3D PANi-graphene-DWNT network becomes higher, creating an extended conjugation PANi-based system that would be expected to show increased electrical conductivity.[32–34]

Figure 2 shows how graphene, DWNT, and PANi are oriented in these thin films. atomic force microscopy (AFM), scanning electron microscopy (SEM), and transmission electron microscopy (TEM) were used to observe the morphology of a 2 QL film. The AFM image clearly shows that DWNTs were interwoven with each other, creating nanotube bundles due to their high concentration. The addition of surfactants allows DWNT and graphene to be exfoliated and uniformly dispersed in the LbL thin films, forming a 3D network with polymer-like entanglements of nanotubes and graphene platelets. This nanoscale morphology facilitates the formation of a highly electrically conductive network. SEM images suggest that individual DWNT and their bundles randomly intertwine together to form a well-dispersed network (Figure 2b). This image also shows multiple nanotubes acting as conductive bridges connecting adjacent graphene sheets. As the inset in Figure 2b shows, two individual graphene platelets are overlaid with DWNT bundles. In films with more QL, graphene platelets are increasingly overlapping, making it difficult to find

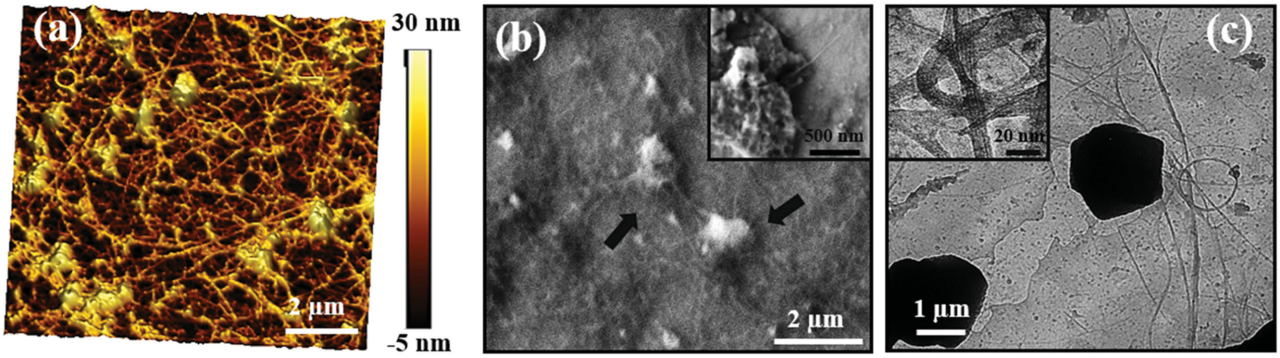

Figure 2. a) AFM 3D height image, b) SEM, and c) TEM images of a 2QL film. The insets in the SEM and TEM images show higher resolution graphene platelets and DWNT, respectively. The arrows indicate graphene in the film.

distinct boundaries of individual platelets. TEM provides more detailed information about the PCN structure (Figure 2c). Two overlapped graphene sheets (average diameter 1–1.5 μm) are surrounded by a PANi–DWNT matrix, where the PANi and DWNT morphology is an interconnected network. The inset in Figure 2c indicates that the DWNT are aligned in the film. Most of the DWNT surface appears to be tightly coated by PANi along the length direction, implying strong binding between DWNT and PANi. The cross-sectional TEM image identifies long straight strands of nanotubes crossing the film in all directions and also verifies the film thickness measured by profilometry (Figure S1, Supporting Information). The π-bonded surface of the DWNTs interacts strongly with the conjugated structure of PANi (Figure S2, Supporting Information), which facilitates the deposition of polymer at the surface of the nanotubes, forming a tubular coating layer that results in an increase of the diameter of PANi–DWNT bundles (of up to 30–50 nm). PANi-covered DWNT and graphene contacts within this network offer a pathway for electron transport and are believed to greatly affect the electrical properties of these PCN films.

Sheet resistance of the BL and QL PCNs was measured by a four-point probe apparatus and then converted to electrical conductivity by multiplying sheet resistance and film thickness, as shown in **Figure 3**a,b. In order to understand the synergistic improvement of the electrical conductivity in PANi/graphene/PANi/DWNT QDs, the conductivity of the individual BL systems must first be evaluated. The sheet resistance of PANi/graphene and PANi/DWNT decreased as a function of BLs deposited. Because a more continuous 3D network is created with a greater number of layers, providing more efficient electron transport, PANi/DWNT achieved conductivity as high as 840 S cm^{-1} at 40 BL (250 nm thick, with a sheet resistance of 47.1 Ω sq^{-1}). In sharp contrast, 40 BL PANi/graphene has a relatively low conductivity of 0.14 S cm^{-1}. The low electrical conductivity relative to PANi/DWNT is most likely due to the fact that this system has a relatively low loading of graphene (35.3 wt% by QCM), so conductivity results primarily from PANi. The electrical conductivity of PANi/DWNT is three orders of magnitude higher than that of PANi/graphene, which suggests that DWNT creates a more efficient percolating network compared to the graphene platelets.[35] The sheet resistance of PANi/graphene/PANi/DWNT significantly decreased to as low as 19.8 Ω sq^{-1} at 40 QL, which is likely due to increased film thickness and connectivity of the graphene/DWNT network. With increasing number of cycles, more nanotubes and graphene are effectively utilized, bridging a continuous 3D polymer nanocomposite network and providing more efficient electron transport. Polymer composites containing graphene or nanotubes become electrically conductive when their concentration is above the percolation threshold.[36] In the QL–PCN, electrical conductivity increases up to 1080 S cm^{-1} as the number of cycles increases to 40, and then achieves steady state (1025 and 1015 S cm^{-1} at 50 and 60 QLs, respectively). This suggests that polymer nanocomposites have a graphene and DWNT concentration above the percolation threshold with a uniform alignment of the 3D network structure.[37] The conductivity of these QL PCN is lower than CNT-based films assembled with vacuum filtration (6700 S cm^{-1}),[38] spraying (5500 S cm^{-1}),[39] chemical vapor deposition (2026 S cm^{-1}),[40] and transfer printing (2000 S cm^{-1}),[41] but higher than some nanotube-based LbL assemblies.[42,43]

The Seebeck coefficient and power factor of the BL and QD systems were measured as a function of the number of layers deposited, as shown in Figure 3c,d. The Seebeck coefficient of all films is positive, indicating *p*-type transport. Both PANi/graphene and PANi/DWNT exhibited a modest increase in *S* with thickness, attaining 25 and 95 μV K^{-1} at 40 BL, respectively. The calculated power factor ($PF = S^2\sigma$) of PANi/DWNT is as high as 765 μW m^{-1} K^{-2}, which is competitive with the best organic TE materials.[44–46] PANi/graphene/PANi/DWNT QL films achieved a Seebeck coefficient as high as 130 μV K^{-1} at 40 QL. This film has a power factor of 1825 μW m^{-1} K^{-2}, which is the highest value ever reported for a fully organic TE material.[33,47–49] By fully taking advantage of nanoscale engineering using the LbL approach, the graphene, PANi, and DWNT in the QL films exhibited a strong synergistic effect that surpassed the BL–LbL nanocomposites, without sacrificing the intrinsic electrical properties of the individual carbon components.

The exceptional TE behavior of these PCN thin films (over each component, Table S1, Supporting Information) is attributed to the continuous 3D PANi-wrapped DWNT and graphene network, assembled LbL, as shown in **Scheme 1**a. When the substrate is alternately exposed to each solution, the conductive polymer (i.e., PANi), PSS-stabilized graphene,

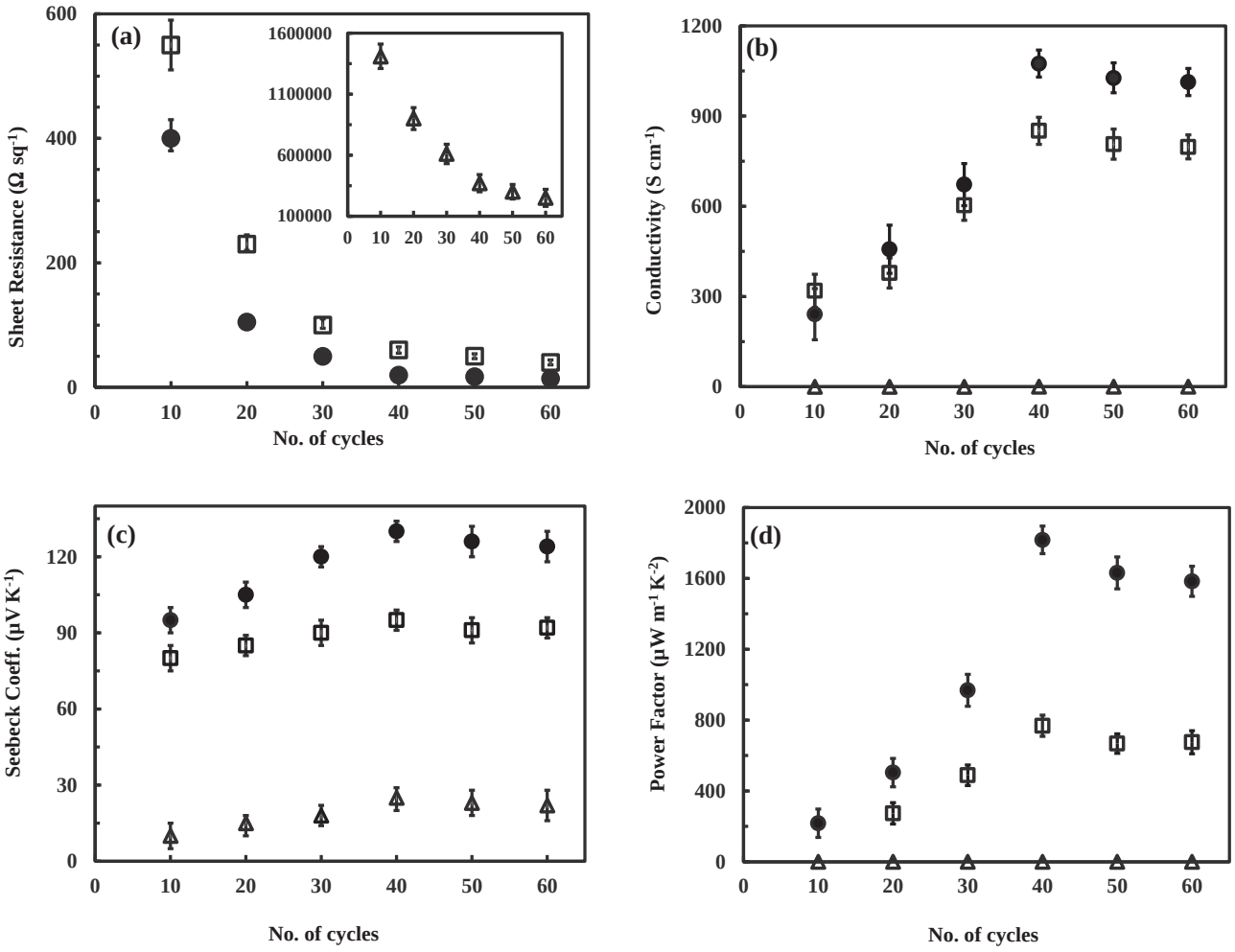

Figure 3. a) Sheet resistance, b) electrical conductivity, c) Seebeck coefficient, and d) power factor of PANi/graphene (open triangles), PANi/DWNT (open squares), and PANi/graphene/PANi/DWNT (filled circles) as a function of bilayers or quadlayers (i.e., cycles) deposited on a PET substrate. Electrical conductivity and power factor of PANi/graphene are shown (Figure S3, Supporting Information).

and SDBS-stabilized DWNT are assembled into a uniformly structured network where each component can retain its individual traits and provide improved TE properties. As more layers are deposited, these nanocomposite thin films become more electrically conductive because the density of the interconnections between polymers and carbon nanoparticles in the layers increases.[37,42,50] For the nanostructured PANi-covered DWNT (Figure S4, Supporting Information), the conjugated structure of PANi grows along the axis and around the outer surface of DWNT bundles through π–π interactions. The electrical conductivity of PANi is dependent on molecular arrangements,[51,52] which was observed by UV–vis (Figure 1c). PANi exhibits a structural rearrangement, from random (ring twisting) in solution to an expanded chain conformation on the surface of DWNT in the deposited film, which in turn increases the effective degree of electron delocalization. This expanded chain conformation allows for better electron flow in the DWNT network, improving carrier mobility, and results in an increase of both electrical conductivity and Seebeck coefficient through adjustment of the hopping barrier.[11,53] In typical bulk inorganic TE materials, increasing carrier concentration usually results in a decrease in the Seebeck coefficient with increasing electrical conductivity.[54] In the present films, the molecular reordering of PANi chains shows an unexpected improvement in charge carrier mobility that leads to an increase in S and σ simultaneously. As others have observed this same phenomenon,[11,32–34,55] the simultaneous increase in both S and σ is believed to primarily come from the carrier mobility enhancement. Charge carrier mobility and carrier concentration for 20, 30, and 40 cycles are summarized in Table S2 (Supporting Information). Mobility more than doubles with increasing layers, while carrier concentration remains nearly constant.

Although not clearly observed, it is likely that the end fragments of the PANi-covered DWNT bridge adjacent graphene nanoplatelets along their surfaces (Figure 2 and Scheme 1b). This hybrid network provides synergistic improvement in the electrical conductivity. With added layers, an extended network of conducting graphene pathways is created, which dominates over the contribution of the PANi/DWNT bridges. In these PCN LbL films, the carriers pass through PANi (or SDBS)-covered DWNT interfaces and graphene sheets. If the low-energy carriers are strongly scattered, and the carriers with higher energy

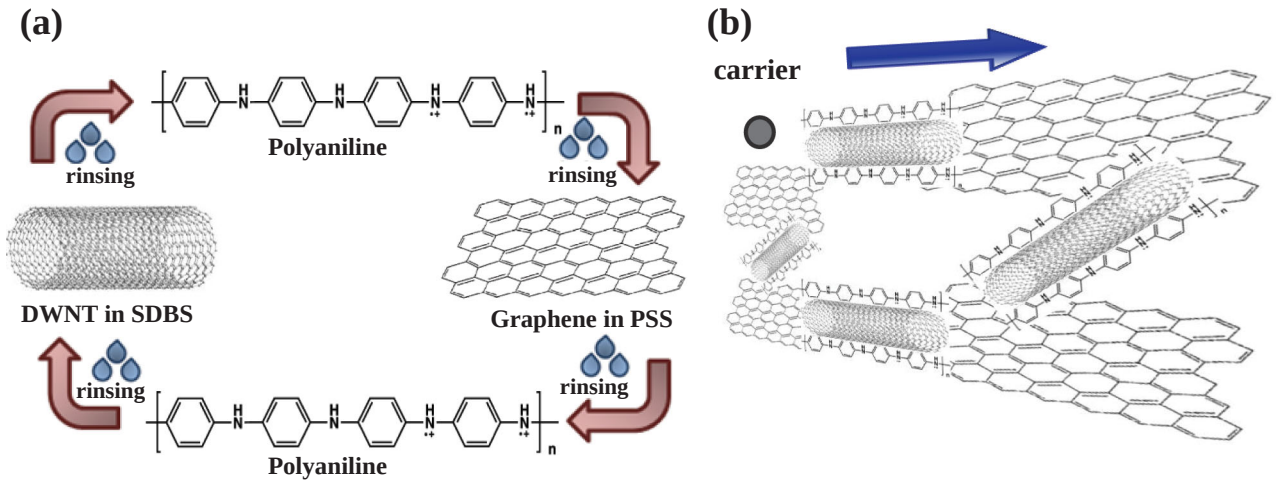

Scheme 1. Schematic representation of the layer-by-layer (LbL) self-assembly procedure (a) and carrier transport in the PANI/graphene/PANi/DWNT nanocomposite multilayers (b).

are unaffected, the mean carrier energy in electronic transport and the Seebeck coefficient will be increased.[12,56] These nanocomposite films are too thin (≈470 nm) to accurately measure thermal conductivity, making it impossible to calculate a realistic TE figure-of-merit (*ZT*). With that said, the PANi/graphene/PANi/DWNT QDs form many nanointerfaces, which likely scatter phonons and decrease thermal conductivity.[2] Most bulk nanocomposites exhibit low thermal conductivity,[57] but oriented films can exhibit much higher values.[58] *ZT* for the present films could be anywhere from 0.05 to 1.8 at room temperature (base on κ ranging from 0.3 to 10 W m^{-1} K^{-1}), but lower thermal conductivity (and higher *ZT*) is expected for the reasons just mentioned.

In summary, PANI/graphene/PANi/DWNT nanocomposites with ordered molecular structure have been prepared using LbL deposition. The maximum power factor of the 40 QL–PCN reached 1825 μW m^{-1} K^{-2}, which is the highest value ever reported for a completely organic material. This exceptional performance is attributed to synergy within the 3D conjugated network, with PANi-covered DWNT bridging gaps between graphene sheets, which increases the electrical conductivity and Seebeck coefficient due to improved carrier mobility. One limitation in assembling polymer nanocomposites with the LbL approach is long deposition times and the large number of layers needed to make thick enough free-standing films. Spin-coating,[59] spraying,[60] or EPD[61] (electrophoretic deposition)-assisted LbL methods could provide an opportunity to circumvent both of these problems. In all respects, the LbL approach reported here provides a unique way to fabricate nanostructured hybrid composites with great potential to improve the performance of TE-driven devices. These water-based nanocoatings could be painted or printed anywhere there is a thermal gradient present (e.g., exhaust pipes, cell phones, or even clothing that harnesses body heat).

Supporting Information

Supporting Information is available from the Wiley Online Library or from the author.

Acknowledgements

The authors gratefully acknowledge financial support from the US Air Force Office of Scientific Research (Grant No. FA9550–13–1–0085).

Received: December 15, 2014
Revised: March 11, 2015
Published online: April 7, 2015

[1] Total Electric Power Industry Summary Statistics 2012, http://www.eia.gov/electricity/annual, accessed: December 2014.
[2] L. E. Bell, *Science* **2008**, *321*, 1457.
[3] A. J. Minnich, M. S. Dresselhaus, Z. F. Ren, G. Chen, *Energy Environ. Sci.* **2009**, *2*, 466.
[4] T. M. Tritt, H. Boettner, L. Chen, *MRS Bull.* **2008**, *33*, 366.
[5] T. C. Harman, P. J. Taylor, M. P. Walsh, B. E. Laforge, *Science* **2002**, *297*, 2229.
[6] N. Dubey, M. Leclerc, *J. Polym. Sci., Part B: Polym. Phys.* **2011**, *49*, 467.
[7] Y. Q. Cao, X. B. Zhao, T. J. Zhu, X. B. Zhang, J. P. Tu, *Appl. Phys. Lett.* **2008**, *92*, 143106.
[8] X. A. Yan, B. Poudel, Y. Ma, W. S. Liu, G. Joshi, H. Wang, Y. C. Lan, D. Z. Wang, G. Chen, Z. F. Ren, *Nano Lett.* **2010**, *10*, 3373.
[9] Y. Pei, A. LaLonde, S. Iwanaga, G. Snyder, *Energy Environ. Sci.* **2011**, *4*, 2089.
[10] F. J. DiSalvo, *Science* **1999**, *285*, 703.
[11] Q. Yao, L. D. Chen, W. Q. Zhang, S. C. Liufu, X. H. Chen, *ACS Nano* **2010**, *4*, 2445.
[12] C. Meng, C. Liu, S. Fan, *Adv. Mater.* **2010**, *22*, 535.
[13] B. Abad, I. Alda, P. Diaz-Chao, H. Kawakami, A. Almarza, D. Amantia, D. Gutierrex, L. Aubouy, M. Martin-Gonzalex, *J. Mater. Chem. A.* **2013**, *1*, 10450.
[14] Y. Y. Wang, K. F. Cai, J. L. Yin, Y. Du, X. Yao, *Mater. Chem. Phys.* **2012**, *133*, 808.
[15] K. Zhang, M. Davis, J. Qiu, L. Hope-Weeks, S. Wang, *Nanotechnology* **2012**, *23*, 385701.
[16] G. P. Moriarty, J. H. Whittemore, S. A. Sun, J. W. Rawlins, J. C. Grunlan, *J. Polym. Sci., Part B: Polym. Phys.* **2011**, *49*, 1547.
[17] Z. Zhang, G. Chen, H. Wang, X. Li, *Chem. Asian J.* **2015**, *10*, 149.
[18] G. Decher, J. B. Schlenoff, *Multilayer Thin Films: Sequential Assembly of Nanocomposite Materialsm*, Wiley, Weinheim, Germany **2012**.

[19] K. Ariga, Q. Ji, J. P. Hill, Y. Bando, M. Aono, *NPG Asia Mater.* **2012**, *4*, e17.
[20] J. Borges, J. F. Mano, *Chem. Rev.* **2014**, *114*, 8883.
[21] Y.-H. Yang, L. Bolling, M. A. Priolo, J. C. Grunlan, *Adv. Mater.* **2013**, *25*, 503.
[22] J. Zhu, B. S. Shim, M. D. Prima, N. A. Kotov, *J. Am. Chem. Soc.* **2011**, *133*, 7450.
[23] P. Joo, K. Jo, G. Ahn, D. Voiry, H. Y. Jeong, S. Ryu, M. Chhowalla, B.-S. Kim, *Nano Lett.* **2014**, *14*, 6456.
[24] J. Paloheimo, K. Laakso, H. Isotalo, H. Stubb, *Synth. Met.* **1995**, *68*, 249.
[25] F. Rivadulla, C. Mateo-Mateo, M. A. Correa-Duarte, *J. Am. Chem. Soc.* **2010**, *132*, 3751.
[26] J. Lynch, M. Kotiuga, V. V. T. Doan-Nguyen, W. L. Queen, J. D. Forster, R. A. Schlitz, C. B. Murray, J. B. Neaton, M. L. Chabinyc, J. J. Urban, *ACS Nano* **2014**, *8*, 10528.
[27] J. Martin, G. S. Nolas, *Appl. Phys. Lett.* **2007**, *90*, 222112.
[28] B. Poudel, Q. Hao, Y. Ma, Y. Lan, A. Minnich, B. Yu, X. Yan, D. Wang, A. Muto, D. Vashaee, X. Chen, J. Liu, M. S. Dresselhaus, G. Chen, Z. Ren, *Science* **2008**, *320*, 634.
[29] J. H. Cheung, W. B. Stockton, M. F. Rubner, *Macromolecules* **1997**, *30*, 2712.
[30] G. Li, L. Jiang, H. Peng, *Macromolecules* **2007**, *40*, 7890.
[31] S. Bhadra, D. Khastgir, N. K. Signha, J. H. Lee, *Prog. Polym. Sci.* **2009**, *34*, 783.
[32] Q. Yao, Q. Wang, L. Wang, Y. Wang, J. Sun, H. Zeng, Z. Jin, X. Huang, L. Chen, *J. Mater. Chem. A* **2014**, *2*, 2634.
[33] Y. Zhao, G.-S. Tang, Z.-Z. Yu, J.-S. Qi, *Carbon* **2012**, *50*, 3064.
[34] Y. Du, S. Z. Shen, W. Yang, R. Donelson, K. Cai, P. S. Casey, *Synth. Metals* **2012**, *161*, 2688.
[35] A. Yu, P. Ramesh, X. Sun, E. Bekyarova, M. E. Itkis, R. C. Haddon, *Adv. Mater.* **2008**, *20*, 4740.
[36] S. Kirkpatrick, *Rev. Mod. Phys.* **1973**, *45*, 574.
[37] Y. T. Park, A. Y. Ham, J. C. Grunlan, *J. Phys. Chem. C.* **2010**, *114*, 6325.
[38] Z. C. Wu, Z. H. Chen, X. Du, J. M. Logan, J. Sippel, M. Nikolou, K. Kamaras, J. R. Reynolds, D. B. Tanner, A. F. Hebard, A. G. Rinzler, *Science* **2004**, *305*, 1273.
[39] H. Z. Geng, K. K. Kim, K. P. So, Y. S. Lee, Y. Chang, Y. H. Lee, *J. Am. Chem. Soc.* **2007**, *129*, 7758.
[40] W. J. Ma, L. Song, R. Yang, T. H. Zhang, Y. C. Zhao, L. F. Sun, Y. Ren, D. F. Liu, L. F. Liu, J. Shen, Z. X. Zhang, Y. J. Xiang, W. Y. Zhou, S. S. Xie, *Nano Lett.* **2007**, *7*, 2307.
[41] Y. X. Zhou, L. B. Hu, G. Gruner, *Appl. Phys. Lett.* **2006**, *88*, 123109.
[42] B. S. Shim, Z. Y. Tang, M. P. Morabito, A. Agarwal, H. P. Hong, N. A. Kotov, *Chem. Mater.* **2007**, *19*, 5467.
[43] S. W. Lee, B. S. Kim, S. Chen, Y. Shao-Horn, P. T. Hammond, *J. Am. Chem. Soc.* **2009**, *131*, 671.
[44] C. Yu, K. Choi, L. Yin, J. C. Grunlan, *ACS Nano* **2011**, *5*, 7885.
[45] Y. S. Kim, D. Kim, C. Yu, J. C. Grunlan, *Nano Lett.* **2008**, *8*, 4428.
[46] G. P. Moriarty, J. N. Wheeler, C. Yu, J. C. Grunlan, *Carbon* **2012**, *50*, 885.
[47] T. Park, C. Park, B. Kim, H. Shin, E. Kim, *Energy Environ. Sci.* **2013**, *6*, 788.
[48] O. Bubnova, Z. U. Khan, A. Malti, S. Braun, M. Fahlmawn, M. Berggren, X. Crispin, *Nat. Mater.* **2011**, *10*, 429.
[49] D. Kim, Y. Kim, K. Choi, J. C. Grunlan, C. Yu, *ACS Nano* **2010**, *4*, 513.
[50] R. Ramasubramaniam, J. Chen, H. Y. Liu, *Appl. Phys. Lett.* **2003**, *83*, 2928.
[51] S. Bhadra, D. Khastgir, N. K. Singha, J. H. Lee, *Prog. Polym. Sci.* **2009**, *34*, 783.
[52] P. M. Ajayan, O. Stephan, P. Redlich, C. Colliex, *Nature* **1995**, *375*, 564.
[53] Y. Long, Z. Chen, X. Zhang, J. Zhang, Z. Liu, *Appl. Phys. Lett.* **2004**, *85*, 1796.
[54] Y. Du, S. Z. Shen, W. Yang, R. Donelson, K. Cai, P. S. Casy, *Synth. Metals* **2012**, *161*, 2688.
[55] H. Yan, T. Ohta, N. Toshima, *Macromol. Mater. Eng.* **2001**, *286*, 139.
[56] S. V. Faleev, F. Leonard, *Phys. Rev. B.* **2008**, *77*, 214304.
[57] P. G. Moriarty, D. Sukanta, J. P. King, U. Khan, M. Via, A. J. King, N. J. Coleman, J. C. Grunlan, *J. Polym. Sci., Part B: Polym. Phys.* **2013**, *51*, 119.
[58] V. Singh, L. T. Bougher, A. Weathers, Y. Cai, Y. Bi, T. M. Pettes, A. S. McMenamin, W. Lv, P. D. Resler, R. T. Gattuso, H. D. Altman, H. K. Sandhage, L. Shi, A. Henry, A. B. Cola, *Nat. Nanotechnol.* **2014**, *9*, 384.
[59] P. A. Chiarelli, M. S. Johal, J. L. Casson, J. B. Roberts, J. M. Robinson, H. L. Wang, *Adv. Mater.* **2001**, *13*, 1167.
[60] M. Bruening, D. Dotzauer, *Nat. Mater.* **2009**, *8*, 449.
[61] Y. H. Ko, Y. H. Kim, K. T. Nam, J. H. Park, P. J. Yoo, *Macromolecules* **2011**, *44*, 2866.